Bioconjugate Chemistry

Article

pubs.acs.org/bc

In Vivo Gastric Cancer Targeting and Imaging Using Novel Symmetric Cyanine Dye-Conjugated GX1 Peptide Probes

Jing Xin,[†] Xianghan Zhang,[†] Jimin Liang,*[,†] Limin Xia,[§] Jipeng Yin,[§] Yongzhan Nie,[§] Kaichun Wu,[§] and Jie Tian*[,†,‡]

[†]School of Life Sciences and Technology, Xidian University, Xi'an, Shaanxi 710071, China

[‡]Institute of Automation, Chinese Academy of Sciences, Beijing 100190, China

[§]Institute of Digestive Diseases, Xijing Hospital, The Fourth Military Medical University, Xi'an, Shaanxi 710032, China

Supporting Information

ABSTRACT: To facilitate the translation of cancer fluorescence imaging into clinical practice, the development of stable and highly specific and sensitive targeted fluorescence probes with low toxicity is desirable. GX1, a gastric tumor angiogenesis marker candidate, holds promise in the target-specific delivery of molecular imaging probes for early gastric cancer detection *in vivo*. In this study, we describe the design and synthesis of a series of novel penta-methine cyanine dyes using the symmetric synthesis method and further conjugated the dyes with GX1, allowing specific binding to the vasculature of gastric cancer. This efficient synthetic route can decrease the undesired byproducts, while increasing yield. Furthermore, *in vivo* fluorescence imaging revealed that this novel targeted probe accumulates selectively in the tumor site of SGC-7901 subcutaneous xenograft models. The combination of such novel vasculature-targeted molecular probes with fluorescence imaging technology may improve early detection, metastasis detection, and antitumor angiogenesis therapy for gastric cancer.

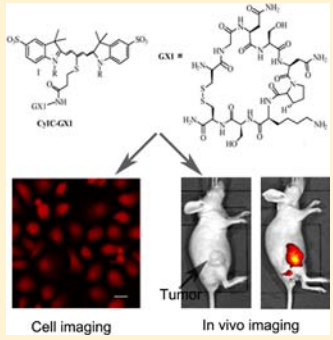

INTRODUCTION

Near-infrared (NIR) fluorescence optical imaging, serving as a novel *in vivo* noninvasive visualization method, has significant impact on early tumor detection and therapy response identification.[1,2] The technology holds many appealing properties, being a low-cost yet high-throughput method with fine temporal resolution, ease of use, and requiring neither ionizing radiation nor radioactive materials. Furthermore, optical imaging in the NIR region provides relatively low tissue absorption and autofluorescence.[3] To take advantage of these benefits, excellent fluorescence probes must be developed.

Cyanine dyes have been widely used as biomedical fluorescence probes for fluorescence labeling because of their small molecular weights, low toxicity, broad spectral tunability, and large molar extinction coefficients.[4−7] Particularly, penta- and hepta-methine cyanine dyes with emission spectra in the 600−900 nm range are useful for *in vivo* optical imaging. The development of these valuable NIR cyanine dyes is very important to facilitate the translation of optical imaging into clinical practice. Recently, the bottleneck points in cyanine dye design are to increase the fluorescence quantum yield and photostability and to establish simple synthesis methods.[8] Cyanine dyes are commonly prepared by an inefficient asymmetrical synthetic route, which results in low yields, formation of undesired byproducts, and tedious purification (see Supporting Information Scheme S1). For this reason, a symmetrical synthetic strategy bearing monofunctional groups on methine chains was developed for cyanine dye synthesis. This notably enriched the cyanine dye family, and the monofunctional groups (amine or carboxylic acid groups) on the methine chains were allowed for bioconjugation.[9,10] The symmetric monocarboxylic acid dyes were developed via the substitution of chloro-atoms by nucleophiles. It is well-known that the chloro group reacts easily with nucleophiles to give the substituted products. This method is widely used for the synthesis of hepta-methine cyanine dyes based on chloro-cyclohexenyl, but seldom used for the synthesis of penta-methine cyanine dyes.[9,10] In an effort to develop novel penta-methine cyanine dyes, we introduce the monochloro-atom into the polymethine chain in this work.

An ideal fluorescence probe should not only have superior chemical and photophysical properties but also suitable chemical functionality for bioconjugation.[11,12] When a fluorescent probe is conjugated with specific ligands, it can accumulate at the target site and improve both the detection sensitivity and specificity of fluorescence molecular imaging.[13,14] Common cancer-specific ligands include small molecules, peptides, proteins, antibodies, antibody fragments, aptamers, and nanoparticles.[15−20] Particularly, low molecular weight peptides are suitable in accomplishing target-specific delivery of molecular imaging probes because of their satisfactory pharmacokinetics, tissue distribution patterns, increased permeability, low toxicity, low immunogenicity, and considerable flexibility in chemical modification.[14]

Received: December 8, 2012
Revised: May 25, 2013
Published: June 1, 2013

Scheme 1. Synthesis of Cyanine Dyes CyI, CyIC, and CyIC-GX1[a]

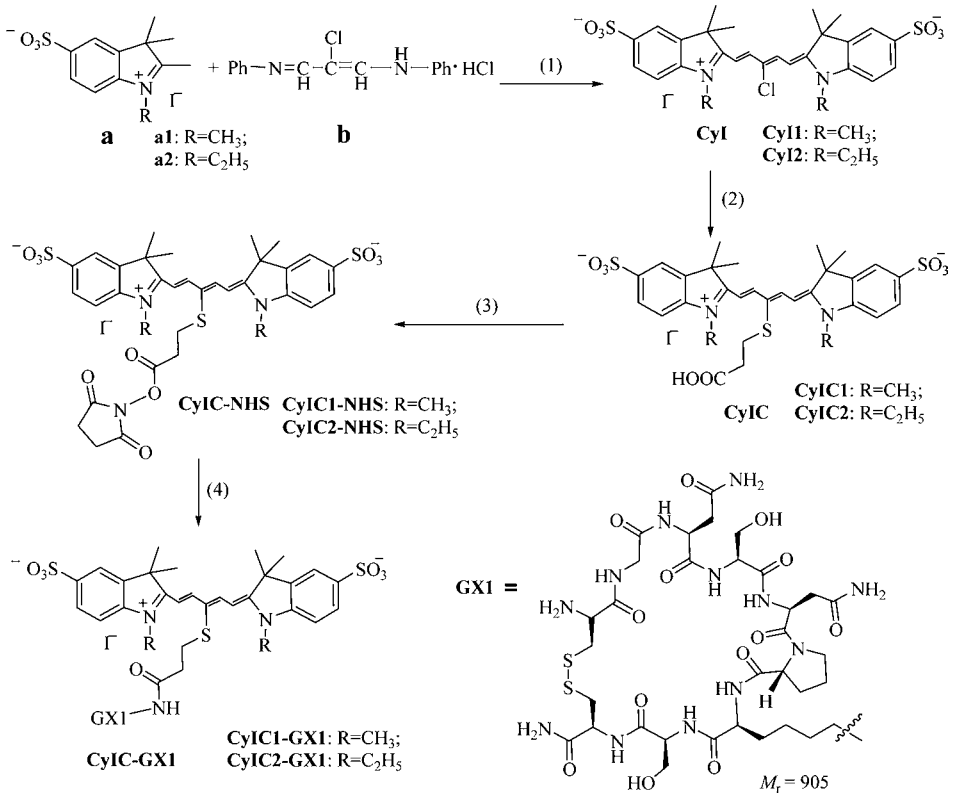

[a]Reaction conditions: (1) Ac_2O, 120 °C, reflux 2 h; (2) 3-mercaptopropionic acid, DMF, RT, 48 h; (3) TSTU, TEA, DMSO, RT, 1 h; (4) TEA, DMSO, RT, overnight.

In cancer imaging, advanced peptide-based fluorescence molecular probes targeting angiogenesis are being intensely investigated to improve tumor metastasis detection and antitumor angiogenesis therapy.[21] Angiogenesis, the formation of new blood vessels from pre-existing vasculature, plays an important role in tumor progression, because it is required for invasive tumor growth and metastasis.[22,23] In this work, we utilize the peptide GX1, a cyclic 9-mer peptide (CGNSNPKSC), as a tumor angiogenesis targeting molecule.[24,25] It has been successfully screened using *in vivo* phage display technology for high affinity and specificity, making GX1 a novel vascular marker candidate for human gastric cancer. Consequently, GX1 targeted probes may contribute to early detection of gastric cancer. Therefore, we chose GX1 as a vascular endothelial cell-specific binding peptide and conjugated it to novel cyanine dyes for gastric cancer targeted imaging.

In the present article, we synthesized a series of symmetric penta-methine cyanine dyes via the symmetric method and evaluated their spectral properties. Gastric cancer cells were used as the *in vitro* model to evaluate cytotoxicity, fluorescence intensity, and nuclear membrane permeability of the novel cyanine dyes and to perform cell imaging. Furthermore, we conjugated the GX1 peptide to these cyanine dyes and imaged gastric tumor vasculature. Fluorescent properties of the conjugate and binding specificity *in vitro* were evaluated based on the coculture model of gastric cancer cells with vascular endothelial cells: Co-HUVEC. It is well-known that tumor angiogenesis is a complex process based upon a series of interactions between tumor cells and endothelial cells. Tumor cells can release growth factors that induce endothelial cells to express specific ligands and their cognate receptors coordinately. Therefore, the *in vitro* Co-HUVEC model acts as a similar scenario to the situation in the solid tumor mass and is used to evaluate the gastric cancer vascular endothelial cell specific molecules *in vitro*.[26] Lastly, we demonstrated the targeting efficacy of these novel symmetric cyanine dye-conjugated GX1 peptide probes *in vivo*.

RESULTS AND DISCUSSION

Synthesis and Characterization of the Dyes. The general synthesis route of dyes is shown in Scheme 1. The asymmetrical route (see Supporting Information Scheme S1) always produces undesired symmetric byproducts with nonfunctional or difunctional groups, which results in low yields of target product (<25%) and tedious purification (always needs HPLC).[27] Therefore, an improved synthesis method for penta-methine cyanine dyes was developed. A series of symmetric penta-methine cyanine dyes **CyI** with a monochloro-atom on the polymethine chain were successfully synthesized with high yields (>50%) via the symmetric method (Scheme 1). The synthetic route produces less byproduct and higher yields of the target product, so the products could be purified by recrystallization using MeOH-H_2O with more ease than the asymmetrical route. Because chloro groups can easily react with nucleophiles, in the next step, the monocarboxylic acid dyes **CyIC** were synthesized by substituting chloro-atoms with 3-mercaptopropionic acid. The crude product was purified by silica gel column chromatography or C18-OPEN column to give 48−51% yield of **CyIC**. Subsequently, **CyIC** were used to conjugate the **GX1** peptide based on the succinimide ester **CyIC-NHS**. The targeted probes **CyIC-GX1** were purified by

dx.doi.org/10.1021/bc3006539 | *Bioconjugate Chem.* 2013, 24, 1134−1143

Prep-HPLC and confirmed by high resolution mass spectroscopy (see Supporting Information Figure S1 and S2), where the peaks at m/z 768.2571 and 782.2749 [M/2 + 2H$^+$] corresponding to **CyIC1-GX1** and **CyIC2-GX1**, respectively, were clearly observed.

Optical Properties of the Dyes. The optical properties of the dyes were tested in different solvents, as shown in Table 1.

Table 1. Optical Properties of Novel Cyanine Dyes

dye	solvent	λ_{abs} (nm)	ε (M^{-1} cm^{-1})	λ_{em} (nm)	Φ_F[a]	Stokes shift (nm)
CyI1	Methanol	645.5	2.30×10^5	668.0	0.18	22.5
	Water	643.5	1.98×10^5	664.2	0.19	20.7
	DMSO	656.0	2.17×10^5	678.8	0.41	22.8
CyI2	Methanol	648.0	2.41×10^5	668.2	0.20	20.2
	Water	646.0	2.28×10^5	666.4	0.18	20.4
	DMSO	657.0	2.19×10^5	678.4	0.42	21.4
CyIC1	Methanol	638.0	2.29×10^5	666.4	0.17	28.4
	Water	633.5	2.04×10^5	658.8	0.17	25.3
	DMSO	645.5	2.05×10^5	671.8	0.38	26.3
CyIC2	Methanol	639.5	2.16×10^5	663.6	0.17	24.1
	Water	636.0	2.20×10^5	661.6	0.16	25.6
	DMSO	648.0	1.96×10^5	670.4	0.40	22.4
Cy5.5	Methanol	675.0	2.33×10^5	700.6	0.24	25.6
	Water	672.0	2.41×10^5	694.0	0.23	22.0
	DMSO	684.0	1.90×10^5	708.6	0.38	24.6

[a]The fluorescence quantum yields of the dyes were determined by the reference standard described in the Supporting Information (Cy5.5 Φ_F = 0.23 in water at 25 °C).

The absorption and emission spectra of the dyes in water are displayed in Figure 1a. The dyes **CyI** and **CyIC** exhibited near-infrared absorption in the range of 633−657 nm with high molar extinction coefficients of (1.96×10^5) to (2.41×10^5) M^{-1} cm^{-1}. The corresponding fluorescence bands had maxima between 658 and 678 nm. Comparing the difference between the position of the absorption and emission maxima for the dyes, the Stokes shifts was about 20 nm. The absorption and emission maxima of **CyIC1** and **CyIC2** was blue-shifted by about 2−10 nm in comparison to **CyI1** and **CyI2**. The quantum yield was in the range of 0.16−0.20 in methanol and water. The compounds exhibited higher quantum yields in dimethyl sulfoxide (DMSO) than in water/methanol (e.g., Φ_F = 0.41 in DMSO compared to Φ_F = 0.18 in methanol for **CyI1**). Aggregation via noncovalent interactions such as $\pi-\pi$ stacking or hydrogen bonding is one of the most common reasons for fluorescence quenching. Weak $\pi-\pi$ stacking interactions and hydrogen bonding of the dyes in aprotic solvent would reduce the fluorescence quenching process, thereby enhancing the fluorescence emission.[28]

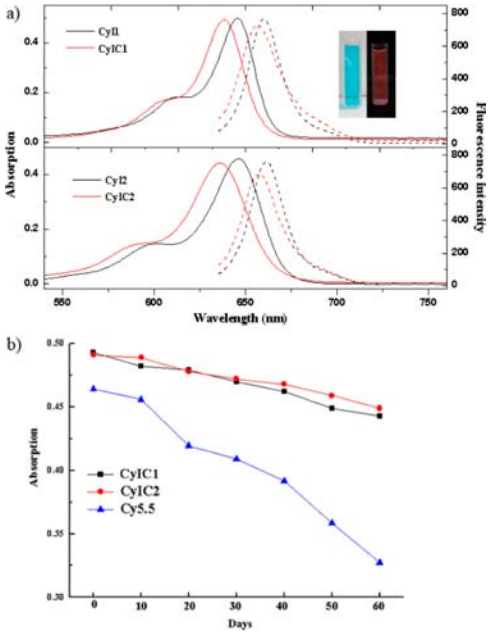

Figure 1. (a) Absorption (—) and fluorescence emission (---) spectra of 2 μM **CyI** (black) and **CyIC** (red) in water at room temperature. (b) Photostability of **CyIC1**, **CyIC2**, and **Cy5.5** in water as measured by the maximum absorption over time after visible light exposure.

The photostability of the dyes was studied in water and compared with commercial probe **Cy5.5** by evaluating absorption spectra exposed to visible light over time. As shown in Figure 1b, both **CyIC1** and **CyIC2** showed excellent photostability. After 60 days of exposure to visible light, **Cy5.5** decreased its maximal absorbance by 30%, but the dyes **CyIC1** and **CyIC2** exhibited only 10% and 9% photofading, respectively. It has been suggested that the poor photostability of polymethine cyanine dyes is caused by singlet oxygen ($^1O_2$) and super oxide anion (O^{2-}) that oxidize excited dye molecules under light irradiation.[29] Compared with Cy5.5, the resistance to oxidation by these radical oxidation species may be improved due to the electron-withdrawing effect of the Cl or S groups, which decrease the electron density on the pentamethine chain of **CyI** and **CyIC**. To investigate this point, theoretical calculations of **CyI1**, **CyIC1**, and **Cy5.5** were performed at the CIS/6-31G* level.[30] From our calculation, the frontier orbitals of **CyI1** are very similar to **CyI2** and **CyIC1** to **CyIC2**. For instance, the transition features, orbital compositions, sketches, and energy values of the molecular orbitals (MOs) of **CyI1** and **CyIC1** are shown in Supporting Information Table S1 and Figure 2. The calculation details and optimized geometries are shown in Supporting Information Figure S3, and the optimized structure with an energy minimum is confirmed by the absence of imaginary frequencies. As shown in Figure 2, HOMO energies of **CyI1**, **CyIC1**, and **Cy5.5** are −5.95 eV, −5.79 eV, and −2.11 eV, respectively, and LUMO energies of **CyI1**, **CyIC1**, and **Cy5.5** are 0.96 eV, 1.14 eV, and 4.14 eV, respectively. Compared with **Cy5.5**, the lower HOMO

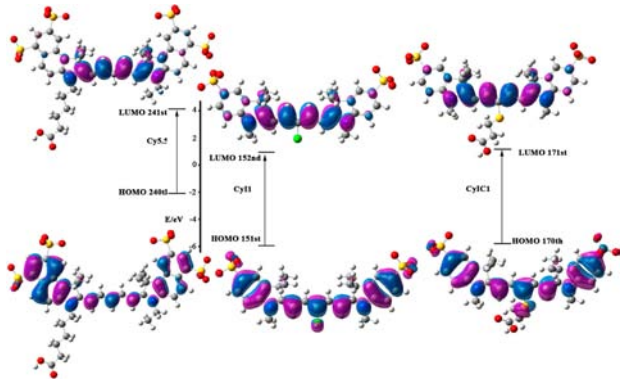

Figure 2. Molecular orbitals of **CyI1**, **CyIC1**, and **Cy5.5** calculated by CIS/6-31G*.

dx.doi.org/10.1021/bc3006539 | Bioconjugate Chem. 2013, 24, 1134−1143

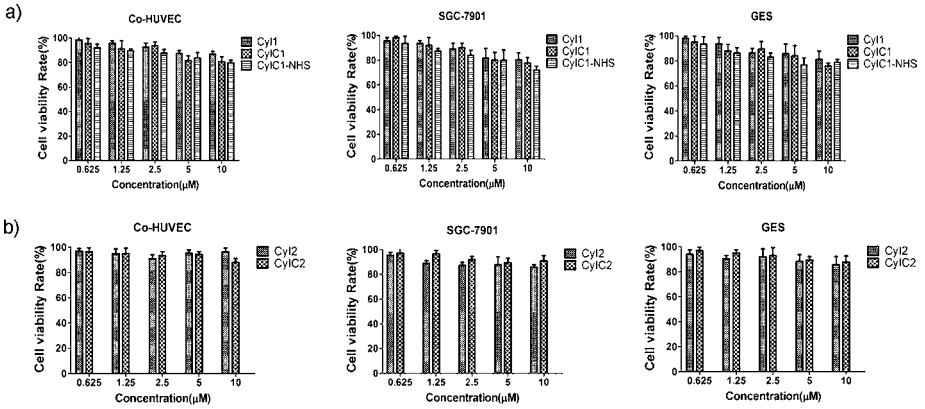

Figure 3. Cytotoxicity of **CyI1** (a) and **CyI2** (b) dyes, as evaluated by the MTT assay. Co-HUVEC, SGC7901, and GES cells were incubated with specific doses of the cyanine dyes for 72 h. Data represent the means ± SD of three independent experiments.

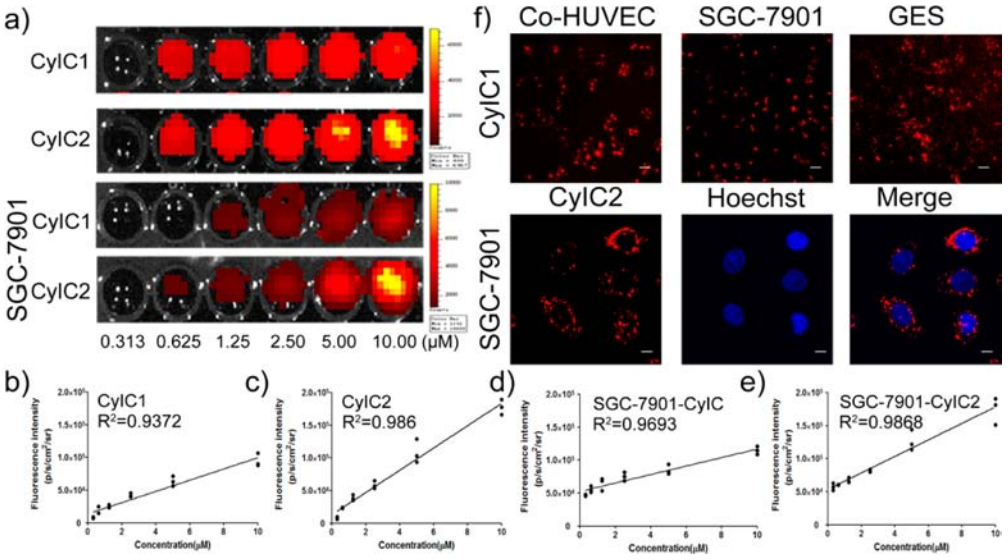

Figure 4. Fluorescence images and microscopy images of **CyIC** cyanine dye. (a) Fluorescence images of **CyIC** dyes only or cells preincubated with **CyIC** dyes at different concentrations. (b–e) Quantified fluorescence intensity showed a strong linear correlation with cyanine dye concentration. Data based on three independent experiments. R^2 indicates the correlation coefficient, which was 0.9372 (b), 0.986 (c), 0.9693 (d), and 0.9868 (d). (f) *In vitro* live cell staining with **CyIC** dyes at a 5 μM concentration. Co-HUVEC, SGC-7901, and GES cells were stained with **CyIC1** cyanine dye for 24 h, and images were obtained by Cellomics ArrayScan V^{TI} 1700 Plus (top), Bar = 125 μm. SGC-7901 cells were stained with Hoechst (nuclear staining) colored in blue and the **CyIC2** cyanine dye (NIR) colored in red. Cells imaged with confocal laser microscopy (bottom), Bar = 6 μm.

and LUMO energy levels of **CyI1** and **CyIC1** cause an increase in the oxidative potential of the dyes, allowing them to be more resistant to photo-oxidation and show better photostability.[31]

Low Cytotoxicity of CyIC Dyes. It is well-known that low cytotoxicity is a stringent requirement for the application of fluorescence dyes *in vitro* or *in vivo*.[11] Therefore, an MTT assay was performed in the present study to evaluate cell toxicity from the cyanine dyes. Co-culture tumor-endothelial cell line Co-HUVEC, gastric cancer cell line SGC-7901, and immortalized fetal gastric epithelial cell line GES were incubated with cyanine dyes with different concentrations for 72 h, and cell viabilities were measured. As shown in Figure 3, after an incubation time of 72 h, the cell viability at the maximum tested concentration of 1×10^{-5} M was more than 80% in the case of **CyIC1** and about 90% in the case of **CyIC2** in all tested cell lines. After increasing the maximum tested concentration, all 50% inhibition concentrations of **CyIC1** and **CyIC2** for Co-HUVEC, SGC-7901, and GES were more than 5×10^{-4} M. The results indicate that the **CyIC1** and **CyIC2** generally exhibit very low cytotoxic effects, and all the cells tested had higher cell viability after being treated with **CyIC2** than **CyIC1** under the same conditions. We also evaluated the cytotoxic effects on other gastric cancer cell lines at different times and compared the cytotoxic effects between **CyIC-NHS** and **Cy5.5-NHS** on SGC-7901 cells with different concentrations for 72 h. Based on these studies, **CyIC** cyanine dyes had weak inhibition effects on MKN28, AGS, and MKN45 cells at 1.25 μM for all incubation times (see Supporting Information Figure S4a). Also, compared to **Cy5.5-NHS**, **CyIC-NHS** had a slightly higher cell vitality on SGC-7901 cell lines, although the cell viabilities of both of them even at the maximum tested concentration of 1×10^{-5} M were more than 70% and the 50% inhibition concentrations of **CyIC1-NHS** and **Cy5.5-NHS** for SGC-7901 cells had no significant difference (see Supporting Information **Figure S4b**). In short, the advantage of using **CyIC** cyanine dyes is that they exhibit low cytotoxic effects on cells *in vitro*.

dx.doi.org/10.1021/bc3006539 | *Bioconjugate Chem.* 2013, 24, 1134–1143

Fluorescence Imaging and Cell Imaging *in Vitro* of CyIC Dyes. To evaluate the fluorescence properties of **CyIC** dyes, a fluorescence imaging system and microscopy were used. First, fluorescence signals from different concentrations of **CyIC** dyes were tested by fluorescence imaging. The intense fluorescence signal could be observed as low as 0.625 μM of **CyIC** dyes, and the **CyIC2** dye fluorescence signal was higher compared to **CyIC1** (top of Figure 4a). The quantified fluorescence signal was strongly linearly correlated with the concentration of each well respectively, with a correlation coefficient of 0.9372 for **CyIC1** dye and 0.986 for **CyIC2** dye (Figure 4b and c). Second, we tested the uptake and accumulation of **CyIC** dyes in cells. SGC-7901 cells after being incubated with **CyIC** dyes at different concentrations (0.313, 0.625, 1.25, 2.5, 5, and 10 μM) for 1 h were imaged on the fluorescence imaging system. As shown at the bottom of Figure 4a,d,e, the fluorescence signals emitting from the cells increased as the concentration increased. A linear fitting was also performed after collecting the fluorescence intensity of SGC-7901 cells incubated with **CyIC1** and **CyIC2** dyes, and the correlation coefficients were 0.9693 and 0.9868, respectively. This revealed that **CyIC** dyes could be accumulated in cells. We then evaluated intracellular locations of retained **CyIC** dyes. Co-HUVEC, SGC-7901, and GES cells were incubated with 5×10^{-6} M **CyIC1** dye and recorded by Cellomics ArrayScan V^{TI} 1700 Plus. The majority of the cells showed intense cytoplasmic staining. Nuclear staining was also observed in a portion of cells (top of Figure 4f). SGC-7901 cells prestained with 5×10^{-6} M **CyIC2** were recorded by confocal laser microscopy and also exhibited intense cytoplasmic staining in cells (bottom of Figure 4f).

Uptake and Accumulation *in Vivo* of CyIC Dyes. Based on our previous experiments, **CyIC2** had lower cytotoxicity and higher fluorescence intensity than **CyIC1**. Therefore, all follow-up experiments are limited to **CyIC2**. In order to study the dye retention status *in vivo*, NIR fluorescence images of **CyIC2** dyes were acquired after subcutaneous injection of 2×10^6 cells preincubated with 5 μM of dye for 1 h. As shown in Figure 5a,b, the fluorescence signals can be clearly visualized for at least 3 days. Fluorescence intensity was quantified at regions of interest (ROI) that encompassed the injection site. The cellular uptake reached a maximum at 6 h postinjection. The fluorescence signals were washed out slowly over time, indicating that **CyIC2** had high uptake and retention in cells. We also observed no toxicity of the **CyIC2** dye in the nude mice. Toxic signs, such as weight loss, scruffy and rough hair, and lethargic behavior, were not found in the nude mice one week after the **CyIC2** dye injection. Further, major organs were extracted at the end point, and pathology examination was carried out by hematoxylin and eosin (H&E) staining. There were no significant lesions in any organs (see Supporting Information Figure S5). Overall, the data on **CyIC2** indicate the possibility of having continuous noninvasive observation *in vivo* for a long time.

Tissue distribution studies were performed in normal athymic nude mice after intravenous injection of 2×10^{-6} M dyes *in vivo*. As shown in Figure 5c and d, **CyIC2** accumulated mainly in the liver, kidneys, and lungs at 6 h postinjection and cleared from all vital organs at 96 h postinjection. The imaging results demonstrate that the dye clearance from the organs was in a time-dependent manner, and **CyIC2** metabolites cleared mainly through the liver and kidneys.

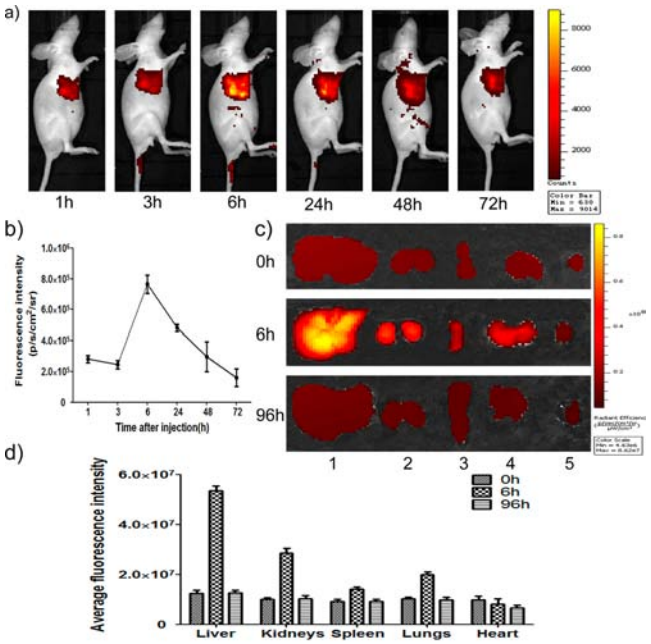

Figure 5. Time course studies of **CyIC** cyanine dye *in vivo* and its metabolites *in vivo*. (a) *In vivo* fluorescence imaging of SGC7901 cells preincubated with cyanine dye implanted into nude mice by subcutaneous injection. The signals could be clearly visualized for at least 3 days and reached the maximum at 6 h. (b) The total fluorescence intensity was quantified by ROI over time. **CyIC** cyanine dyes displayed high uptake, long retention time, and slow clearance. (c) Major organs were dissected at 0, 6, and 96 h after being injected with 2×10^{-6} M cyanine dyes and subjected to fluorescence imaging (1 liver, 2 kidneys, 3 spleen, 4 lungs, 5 heart). (d) Tissue distribution of **CyIC** at 0, 6, and 96 h. **CyIC** metabolites were mainly in the liver and kidneys.

Targeted Affinity of CyIC-GX1 *in Vitro*. To validate the potential applications of **CyIC** dyes, targeted fluorescence probes, **CyIC-GX1**, were synthesized in this study. The fluorescence properties and targeting ability of **CyIC2-GX1** were examined by confocal laser microscopy and flow cytometry. As shown in Figure 6a, fluorescence signals from cellular cytoplasmic and nuclear regions could be easily detected in Co-HUVEC cells. The bright fluorescence and high specific staining reveal that these **CyIC** dyes have great potential in fluorescence labeling. The fluorescence profiles and binding percentages of the cells are shown in Figure 6b. Compared to GES cells, the binding percentages of **CyIC2-GX1** to Co-HUVEC cells were more than 2-fold higher (85.9% vs 39.1% at a high concentration and 57.8% vs 26% at a low concentration), and the percentage of cell binding was dependent on the concentration of **CyIC-GX1**. To further validate that GX1 is critical for the targeted fluorescence probes' specificity, an *in vitro* blocking experiment was performed using unlabeled GX1. Co-HUVEC cells, pretreated with 5×10^{-6} M unlabeled GX1 and incubated with 5×10^{-6} M **CyIC-GX1**, were imaged by confocal laser microscopy and quantified by flow cytometry. By increasing the blocking time of GX1, the fluorescence signal and the binding percentages of cells was obviously decreased (Figure 6c). The results also reveal that Co-HUVEC successfully mimicked tumor vasculature endothelial cells *in vitro*, and GX1 bound specifically to gastric cancer vasculature.

dx.doi.org/10.1021/bc3006539 | *Bioconjugate Chem.* 2013, 24, 1134−1143

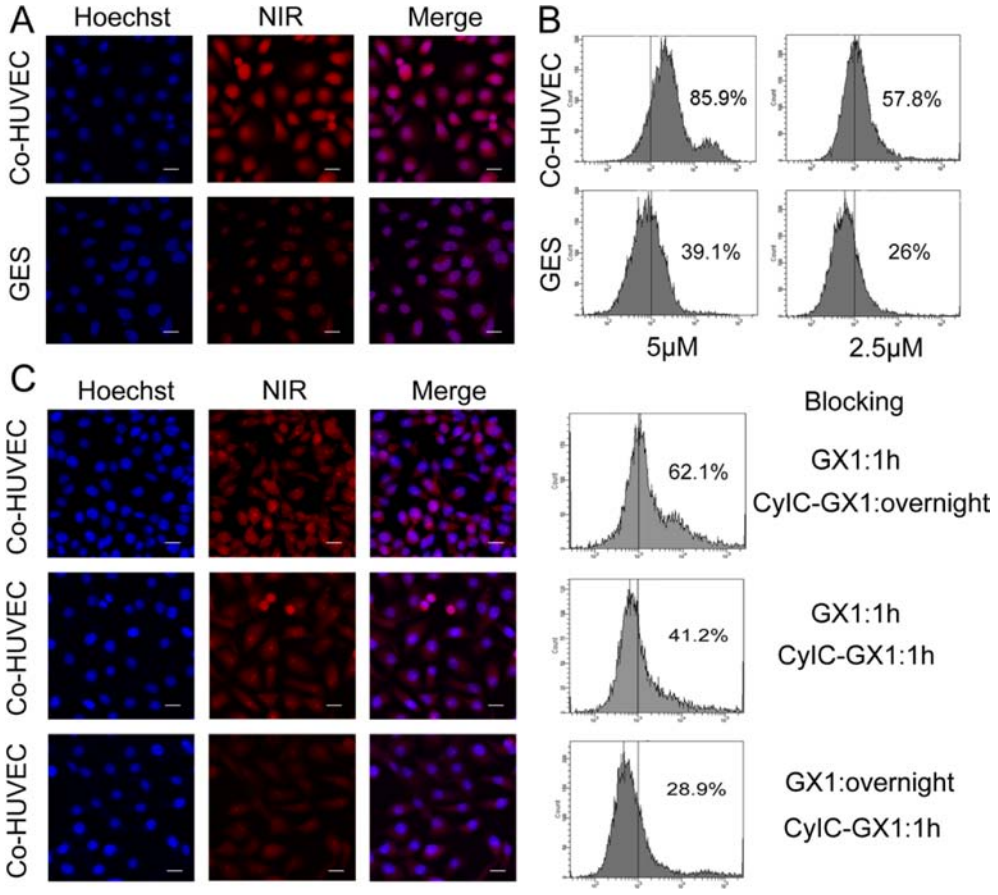

Figure 6. Targeting specificity of **CyIC-GX1** *in vitro*. (a) Confocal laser microscopy of Co-HUVEC and GES cells incubated with targeted fluorescence probe, **CyIC-GX1**, at a 5 μM concentration. Cells were stained with Hoechst (nuclear staining) colored in blue, and the **CyIC** cyanine dye (NIR) colored in red. All of the images were acquired at 600× magnification. The scale bar represents 20 μm. (b) Cell binding affinity of **CyIC-GX1** was evaluated by flow cytometry. Co-HUVEC and GES cells were treated with **CyIC-GX1** at a concentration of 5 μM or 2.5 μM **CyIC-GX1** for 1 h and analyzed by flow cytometry. Graphs provide the percentage of binding to cells. (c) Fluorescence imaging and cell binding affinity of **CyIC-GX1** in the blocking experiment. Co-HUVEC cells were treated with 5 μM **CyIC-GX1** after being preincubated with 5 μM unlabeled GX1 at the indicated time.

Fluorescence Imaging of CyIC-GX1 *in Vivo*. To further evaluate the tumor targeting ability and *in vivo* accumulation of **CyIC2-GX1**, fluorescence imaging was acquired after intravenous injection of 5×10^{-6} M **CyIC2-GX1** to SGC-7901 subcutaneous xenograft models. Fluorescence signal from **CyIC2-GX1** was significant at the tumor site and remained there for a long time (Figure 7a). Although fluorescence signal was also observed in normal organs, it was lower compared to the tumor. Fluorescence intensity was quantified at the ROI that encompassed the tumor tissue. The accumulation of **CyIC2-GX1** in the tumor reached a maximum at 16−18 h (Figure 7b). A blocking experiment was also performed to validate the targeting specificity of **CyIC2-GX1** *in vivo*. Mice intravenously injected with 5×10^{-6} M **CyIC2-GX1** only served as a control group, and mice intravenously injected with 20 mg/kg of unlabeled GX1 and then injected with 5×10^{-6} M **CyIC2-GX1** were the blocked group. The fluorescence signal at the tumor site was approximately three times higher in the control group than the blocked group (Figure 7c). Fluorescence images of excised organs indicated that **CyIC2-GX1** accumulated in the tumor and kidneys (Figure 7d). Compared to the blocked group, **CyIC2-GX1** showed excellent tumor uptake with minimal accumulation in other normal organs (Figure 7e).

Furthermore, fluorescence imaging was performed on SGC-7901 subcutaneous xenograft models with 5×10^{-6} M **Cy5.5-GX1** and further compared with **CyIC2-GX1** for specificity. The **Cy5.5-GX1** also exhibited high tumor site uptake and reached maximum fluorescence intensity at 6 h postinjection. Compared to **CyIC2-GX1**, it exhibited rapid tumor targeting at an earlier time point (see Supporting Information **Figure S6a-6b**). Ex vivo fluorescence imaging of major organs showed that **Cy5.5-GX1** accumulated not only in the tumor, but also in the kidneys and stomach (see Supporting Information **Figure S6c-6d**). To compare the specificity of each targeted probe, tumor-to-organ ratios at their maximum uptake period were calculated. **CyIC2-GX1** showed the highest contrast to normal tissues. Its tumor-to-kidneys ratio and tumor-to-stomach were 7.04 ± 3.09 and 11.8 ± 1.25, respectively, while the corresponding values of **Cy5.5-GX1** were 1.06 ± 0.62 and 3.95 ± 1.78, respectively (see Supporting Information **Figure S6e**). The differences in uptake may be caused by the level of normal tissue metabolism of the dye at the maximum uptake period. Finally, the cytotoxicities of **CyIC2-GX1** and **Cy5.5-GX1** *in vivo* were compared. The results show that neither of them led to weight loss and only a few inflmmatory lesions were found in the liver and lung (see Supporting Information **Figure S7**). Thus, both of them have low cytotoxicity *in vivo*. In

dx.doi.org/10.1021/bc3006539 | *Bioconjugate Chem.* 2013, 24, 1134−1143

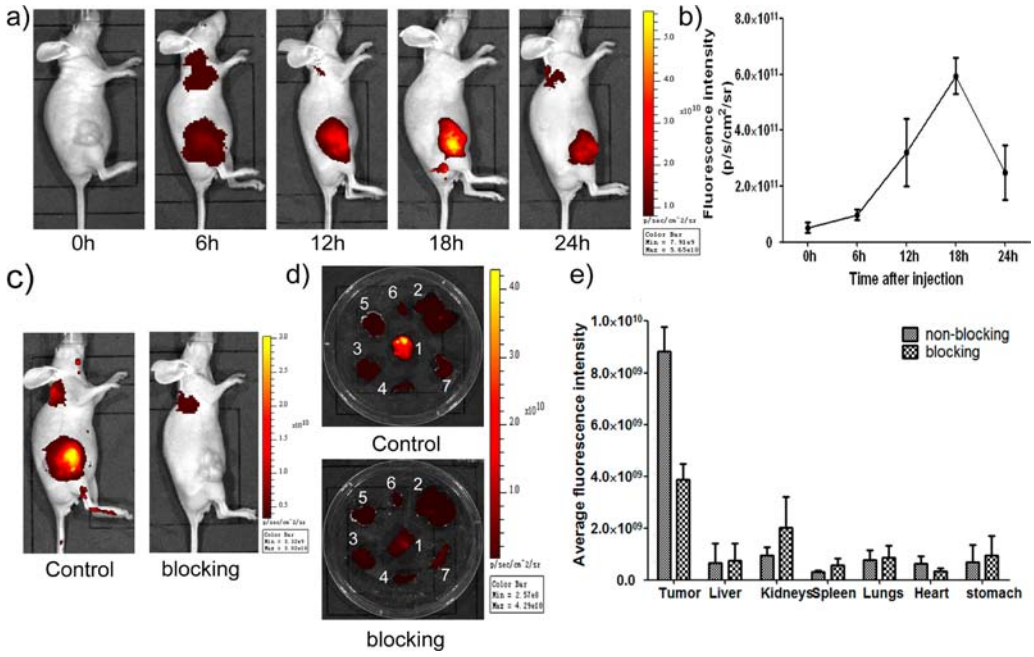

Figure 7. Targeting specificity of **CyIC-GX1** *in vivo*. (a) Fluorescence imaging of subcutaneous tumor-bearing nude mice after intravenous injection with 5×10^{-6} M **CyIC-GX1**. (b) Quantified fluorescence signal emitted from the tumor tissue over time. The accumulation of **CyIC-GX1** in the tumor reached a maximum at 16−18 h. (c) Fluorescence images comparing SGC-7901 subcutaneous xenograft models after being injected with **CyIC-GX1** only (control) or injected with 20 mg/kg of unlabeled GX1 and then injected with **CyIC-GX1** (blocking) at 24 h postinjection. (d) Fluorescence images of excised organs (1 tumor, 2 liver, 3 kidneys, 4 spleen, 5 lungs, 6 heart, 7 stomach) collected from a mouse in the nonblocked group (only injected with **CyIC-GX1**) and blocked group (injected with unlabeled GX1 and **CyIC-GX1**), respectively. (e) The fluorescence intensity analysis of excised organs from the blocked and control groups.

general, the results suggest that **CyIC2-GX1** is an excellent target-specific molecular probe and may contribute to gastric tumor metastasis detection and antitumor angiogenesis therapy by noninvasive targeting molecular imaging.

■ CONCLUSIONS

In this study, a series of novel penta-methine cyanine dyes were synthesized by the symmetric synthesis method. This efficient synthetic route for the cyanine dye could decrease the undesired byproducts and increase yield. The obtained fluorophores exhibited high photostability, nuclear membrane permeability, little toxicity, and bright fluorescence intensity. Furthermore, the angiogenesis-targeted molecular probes, **CyIC-GX1**, were found to be suitable for *in vivo* gastric cancer targeting and imaging. These probes can image tumor vasculature with high specificity and sensitivity with fast and selective accumulation to the tumor tissue. Such targeted, fluorescent probes provide a promising method for highly selective detection of gastric cancer.

■ EXPERIMENTAL SECTION

Materials and Measurements. All materials and solvents were purchased from Sigma-Aldrich or TCI and used without additional purification. The solvents were analytical grade reagents. TLC (thin layer chromatography) silica gel 60 RP-18 with a F_{254} indicator was purchased from Merck. C18-OPEN silica gel (75 μm) for column chromatography was offered by COSMOSIL. The GX1 peptide was obtained from the State Key Laboratory of Cancer Biology, the Institute of Digestive Diseases, Xijing Hospital, and the Fourth Military Medical University. It was stored at −20 °C and dissolved in PBS on the day of use. MTT was obtained from Sigma-Aldrich.

^{1}H NMR and ^{13}C NMR spectra were recorded at 400 MHz using a Varian Inova-400 spectrometer, and chemical shifts were reported relative to the internal Me_4Si. HRMS spectra were obtained with a Bruker micrOTOF-Q II instrument. The absorption spectra were recorded on a Shimadzu UV-2450 UV−vis spectrometer using water, DMSO, methanol, and ethanol as solvents, each at a concentration of 10^{-5} M in 1 cm quartz cells. Fluorescence measurements were carried out at room temperature on a Hitachi F-4500 spectrofluorometer in 1 cm quartz cells. Excitation maximum was fixed by 3D-fluorescence spectra. The dyes were purified by high-performance liquid chromatography (HPLC) on a Waters 2545 prep LC instrument. An Olympus FV 10i confocal fluorescent microscope and Thermo Cellomics ArrayScan V^{TI} 600 Plus were used in the imaging experiments. *In vitro* and *in vivo* fluorescence imaging was performed on the IVIS Kinetic imaging system. BD FACSCanto flow cytometry was used to detect binding affinity.

Synthesis and Characterization. *Cyanine Dye* ***CyI1.*** Indole quaternary iodide salts **a1** (5 mmol, 2.1 g) and α-chloroprop malonaldehyde dianil hydrochloride **b** (2.5 mmol, 0.7 g) were dissolved in 45 mL acetic anhydride. The reaction was heated under reflux for 2 h. Solvent was evaporated under vacuum, and the crude product was purified by recrystallization from MeOH:H_2O three times to afford **CyI1** as a blue solid (1.9 g, 50% yield). **CyI1** ^{1}H NMR (400 MHz, DMSO-d_6) δ (ppm): 1.73 (s, 12H, $C(CH_3)_2$), 3.68 (s, 6H, NCH_3), 6.29 (d, 2H, J = 13.6 Hz, −CH═), 7.43 (d, 2H, J = 8.0 Hz, ArH), 7.67 (d, 2H, J = 8.0 Hz, ArH), 7.88 (s, 2H, ArH), 8.47 (d, 2H, J = 13.6 Hz, −CH═). ^{13}C NMR (400 MHz, DMSO-d_6) δ (ppm): 26.04, 66.93, 99.72, 110.30, 119.52, 121.90, 125.57, 128.22, 131.24, 142.09, 145.45, 166.54, 174.44. HRMS (ESI, negative

dx.doi.org/10.1021/bc3006539 | *Bioconjugate Chem.* 2013, 24, 1134−1143

mode): calculated M_r = 575.1083 for $C_{27}H_{28}N_2O_6S_2Cl$, found m/z = 575.1108.

Cyanine Dye ***CyI2***. **CyI2** was prepared from **a2** and **b** according to the method described above for the synthesis of **CyI1** to give **CyI2** as a blue solid (2.5 g, 58% yield). **CyI2** ^{1}H NMR (400 MHz, DMSO-d_6) δ (ppm): 1.316 (t, 6H, J = 6.8 Hz, N-β-CH_3), 1.73 (s, 12H, $C(CH_3)_2$), 4.22 (q, 4H, J = 6.8 Hz, N-α-CH_2), 6.32 (d, 2H, J = 13.6 Hz, −CH═), 7.45 (d, 2H, J = 8.4 Hz, ArH), 7.69 (d, 2H, J = 8.4 Hz, ArH), 7.90 (s, 2H, ArH), 8.49 (d, 2H, J = 13.6 Hz, −CH═). ^{13}C NMR (400 MHz, DMSO-d_6) δ (ppm): 11.60, 26.07, 48.15, 49.01, 99.18, 110.24, 119.66, 121.86, 125.71, 140.53, 140.84, 145.48, 147.21, 173.58. HRMS (ESI, negative mode): calculated M_r = 603.1396 for $C_{29}H_{32}N_2O_6S_2Cl$, found m/z = 603.1364.

Cyanine Dye ***CyIC1***. In a dry Parr pressure reactor containing **CyI1** (1.3 mmol, 1 g), 3-mercaptopropionic acid (6 mmol, 0.6 g) was stirred in 20 mL of dry DMF for 48 h. The completion of the reaction was checked by RP-18 TLC, and the mixture was evaporated until dry under vacuum. The crude product was purified on a C18-OPEN column (20−40% MeOH, 0.1% TEA in H_2O) to afford **CyIC1** as a blue solid (0.53 g, 48% yield). **CyIC1** ^{1}H NMR (400 MHz, DMSO-d_6) δ (ppm): 1.73 (s, 12H, CH_3), 2.87−2.90 (m, 4H, CH_2), 3.67 (s, 6H, NCH_3), 6.74 (d, 2H, J = 13.6 Hz, −CH═), 7.41 (d, 2H, J = 8.4 Hz, ArH), 7.66 (d, 2H, J = 8.4 Hz, ArH), 7.86 (s, 2H, ArH), 8.56 (d, 2H, J = 13.6 Hz, −CH═), 12.33 (s, 1H, COOH). ^{13}C NMR (400 MHz, DMSO-d_6) δ (ppm): 8.21, 26.28, 45.26, 48.78, 101.63, 110.07, 119.48, 122.32, 125.52, 140.26, 142.10, 145.27, 155.70, 172.57, 174.54. HRMS (ESI, negative mode): calculated M_r = 645.1405 for $C_{30}H_{33}N_2O_8S_3$, found m/z = 645.1438.

Cyanine Dye ***CyIC2***. **CyIC2** was prepared according to the method described above for **CyIC1**. The crude product was purified by silica gel column chromatography (EtOH/$CHCl_3$/H_2O 2:1.5:0.3), and further purification was carried out on a second C18-OPEN column (20−40% MeOH, 0.1% TEA in H_2O) to afford **CyIC2** as a blue solid (0.58 g, 51% yield). **CyIC2** ^{1}H NMR (400 MHz, DMSO-d_6) δ (ppm): 1.05 (t, 6H, J = 6.8 Hz, N-β-CH_3), 1.73 (s, 12H, $C(CH_3)_2$), 2.73−2.78 (m, 4H, SCH_2CH_2), 4.21 (q, 4H, J = 6.8 Hz, N-α-CH_2), 6.79 (d, 2H, J = 13.6 Hz, −CH═), 7.43 (d, 2H, J = 8.0 Hz, ArH), 7.68 (d, 2H, J = 8.0 Hz, ArH), 7.88 (s, 2H, ArH), 8.58 (d, 2H, J = 13.6 Hz, −CH═), 12.33 (s, 1H, COOH). ^{13}C NMR (400 MHz, DMSO-d_6) δ (ppm): 9.58, 11.71, 26.34, 45.03, 48.90, 101.26, 110.01, 119.65, 123.10, 125.70, 140.50, 140.93, 145.24, 155.92, 161.88, 173.58. HRMS (ESI, negative mode): calculated M_r = 673.1718 for $C_{32}H_{37}N_2O_8S_3$, found m/z = 673.1726.

Conjugate ***CyIC-GX1***. *O*-(*N*-Succinimidyl)-1,1,3,3-tetramethyluronium tetrafluoroborate (TSTU, 5 mg, 0.02 mmol) and TEA (6 μL, 0.04 mmol) were dissolved in 0.5 mL dry DMSO. A 0.5 mL amount of **CyIC** (4 mg, 0.005 mmol) was added to dry DMSO. The reaction mixture was protected from light and stirred at room temperature for 1 h. The completion of the reaction was checked by RP-18 TLC, and the resulting compound **CyIC-NHS** was used for the next step immediately.

GX1 peptide (1 mg) dissolved in 400 μL dry DMSO and TEA (12 μL, 0.08 mmol) was added to the above solvent with **CyIC-NHS**. The reaction mixture was protected from light and stirred at room temperature overnight. The crude mixture was purified on a Prep-HPLC [150 × 19 mm C18 column, 10 mM NH_4HCO_3, and linear gradient from 5% to 40% (15 min) of CH_3CN]. HRMS (ESI, positive mode) of **CyIC1-GX1**: calculated M_r = 1532.4783 for $C_{63}H_{86}N_{15}O_{20}S_5$, found m/z = 768.2571 ($[M_r/2 + 2H^+]$). HRMS (ESI, positive mode) of **CyIC2-GX1**: calculated M_r = 1560.5101 for $C_{65}H_{90}N_{15}O_{20}S_5$, found m/z = 782.2749 ($[M_r/2 + 2H^+]$).

Cell Lines and Cell Culture. Human umbilical vein endothelial cells (HUVECs) were cultured in M200 basal culture medium (Gibco) supplemented with low serum growth supplement (Gibco), 100 U/mL penicillin, and 10 mg/mL streptomycin (complete medium). The human gastric carcinoma cell line SGC7901 and human immortalized fetal gastric epithelial cell line GES were cultured in RPMI1640 (Gibco) culture medium supplemented with 10% fetal bovine serum (Gibco), 100 U/mL penicillin, and 10 mg/mL streptomycin. All cells were cultured in a humidified incubator at 37 °C with 5% CO_2. HUVECs and SGC7901 cell lines were used to establish the tumor-endothelial cell *in vitro* co-culture model. Briefly, SGC7901 cells were cultured in M200 complete medium without low serum growth supplement for 24 h. The culture medium was harvested and centrifuged. The supernatant was harvested and the pellets were discarded. The supernatant was used as the conditioned medium. Then, the conditioned medium and complete medium as described before were mixed well at a ratio of 1:4. HUVEC cells were cultured in mixed medium for 72 h. The Co-HUVECs were harvested and used in experiments as the *in vitro* co-culture model.

MTT Assay. The suitable concentrations of dyes were assessed using MTT to guarantee the minimum toxicity of cells. The suspension containing 5 × 10^3 cells was added to sterile 96-well flat-bottomed plates, and 2 μL aliquots of a series of dyes at different concentrations (0.625 μM to10 μM) were added. Four wells containing only tumor cells were suspended in a mixture solution of 200 μL complete medium and 2 μL DMSO. They were used as the control for investigating cell viability. Four wells containing only the complete medium were used as the blank control for the nonspecific dye reduction. The plates were then incubated at a humidified incubator at 37 °C with 5% CO_2 for 3 days. After incubation, 20 μL of 5 mg/mL MTT solution was added to each well, and then the 96 well plates were incubated for 4 h. The formazan crystal was formed at the bottom of the well. Culture supernatant from the wells was removed. About 150 μL DMSO was added to each well. Shaking the wells for 15 min, the formazan crystal was dissolved completely. The plates were then read on a Microplate Reader with a 490 nm test wavelength.

In Vitro **Fluorescence Imaging.** Fluorescence imaging was performed on the IVIS imaging system and signals were quantified by analysis software Living Image (Xenogen). First, we assessed the fluorescence signals emitted by dyes at different concentrations. About 200 μL of the diluted dye solution was added into sterile PBS in black, clear bottom 96-well plates, and then the plates were imaged with these parameters: exposure time, 50 s; binning, 8; lens aperture [f/stop], 4; field of view, 12.5. Furthermore, *in vitro* fluorescence imaging was performed. Briefly, Co-HUVEC, SGC7901 and GES cell suspensions containing 1 × 10^4 cells were added in black, clear bottom 96-well plates and incubated in a humidified incubator at 37 °C with 5% CO_2 for 24 h. Then, the culture medium was changed and supplemented with different concentrations of dyes from the 96 well plates and incubated in a humidified incubator at 37 °C with 5% CO_2 again. After 1 h, the cells were washed with PBS twice and imaged with these parameters: exposure time, 2 min; binning, 8; lens aperture [f/stop], 2; field of view, 12.5.

***In Vitro* Cell Uptake Study Using CyIC Dyes in Cells.** Co-HUVEC, SGC7901, and GES cells at a density of 1×10^4 were seeded in sterile 96-well flat-bottomed plates and incubated overnight. After the cells attached to the bottom of the culture plates, the cells were washed with PBS and fresh medium supplemented with of 5×10^{-6} M **CyIC1** was added. The plates were incubated at 37 °C with 5% CO_2 for 24 h, and washed twice with PBS again. Images were recorded by Cellomics ArrayScan V^{TI} 600 Plus. SGC7901 cells at a density of 1×10^5 were grown on Bioclean coverslips in 24-well plates and allowed to attach overnight. The cells were washed with PBS and exposed to **CyIC2** at a concentration of 5×10^{-6} M. The coverslips were incubated at 37 °C with 5% CO_2 for 3 h and washed with PBS twice. The cells were fixed with 4% paraformaldehyde fixative for 10 min and rinsed with PBS. Nuclei were stained by Hoechst. Coverslips were mounted on slides with glycerol and imaged by confocal laser microscopy.

***In Vivo* Fluorescence Imaging.** The animal study protocol was in accordance with the Fourth Military Medical University animal protocol. Athymic nude mice (4−6 weeks old weighing 20−25 g) were purchased from the animal center at the Fourth Military Medical University. The cells were harvested at a logarithmic growth phase, separated into a single cell suspension, and incubated with 5×10^{-6} M **CyIC2** dye for 1 h. Approximately 2×10^6 cells were implanted into nude mice via subcutaneous injection. *In vivo* fluorescence imaging was performed on the IVIS imaging system. Identical imaging settings were used for acquiring all images. Briefly, the settings included exposure time, 50 s; binning, 8; lens aperture [f/stop], 4; field of view, 12.5. Fluorescence imaging was continuously observed for a week.

Confocal Laser Microscopy of CyIC-GX1. Co-HUVEC and GES cells with 80% confluence were dissociated with 0.5% trypsin-EDTA and suspended in fresh medium. Approximately 1×10^5 cells were seeded on Bioclean coverslips in 24-well plates and incubated overnight. The cells were washed with PBS, fixed with 4% paraformaldehyde fixative for 10 min, washed twice with PBS, permeabilized with 0.5% Triton X-100 in PBS for 10 min, and again washed twice with PBS. To prevent nonspecific binding, the cells were preincubated in 2% normal goat serum containing 2% bovine serum albumin at 4 °C for 1 h. Then, the cells were incubated with 5×10^{-6} M **CyIC-GX1** for 1 h at 4 °C and washed again with PBS. In the blocking experiment, the Co-HUVEC cells were incubated with 5×10^{-6} M **CyIC-GX1** at different time points followed by pretreatment with unlabeled GX1 for 1 h or overnight at 4 °C and washing with PBS. Hoechst was used for the nuclear staining for 10 min. After drying at room temperature, the coverslips were mounted on slides using the fluorescence mount solution and examined on confocal laser microscopy.

Binding Affinity of GX1 Determined by Flow Cytometry. Co-HUVEC and GES cells were used to detect cell binding affinity of **CyIC-GX1**. The cells were then harvested, washed with PBS twice, and centrifuged again with PBS containing 1% bovine serum albumin. To minimize nonspecific binding, the cells were preincubated in 2% normal goat serum containing 2% bovine serum albumin on ice for 1 h. Then, the cells were centrifuged in 4 °C and incubated with **CyIC-GX1** (5×10^{-6} M and 2.5×10^{-6} M) for 1 h. In the blocking experiment, the Co-HUVEC cells were centrifuged in 4 °C, incubated with 5×10^{-6} M unlabeled GX1 for 1 h or overnight on ice, centrifuged in 4 °C again, and then incubated with 5×10^{-6} M **CyIC-GX1** for 1 h or overnight on ice. After washing three times with iced PBS, the samples were analyzed with flow cytometry.

Fluorescence Imaging with CyIC-GX1 *in Vivo*. After harvesting the SGC-7901 cells at a logarithmic growth phase, a 2×10^6 single cell suspension was implanted into nude mice via subcutaneous injection. When the subcutaneous tumor volume developed to approximately 100 mm^3, fluorescence imaging was acquired after intravenous injection of 5×10^{-6} M **CyIC-GX1** on the IVIS imaging system. Fluorescence imaging was continuously observed for three days. To evaluate the targeting specificity of **CyIC-GX1**, a blocking experiment was also performed. Briefly, mice were divided into two groups randomly. The mice in the nonblocked group were injected with 5×10^{-6} M **CyIC-GX1** and then imaged. The mice in the blocked group were injected with 20 mg/kg of unlabeled GX1, injected with 5×10^{-6} M **CyIC-GX1** after 30 min, and imaged. In the end, the tumors, tissues, and organs were dissected and also imaged.

■ ASSOCIATED CONTENT

Ⓢ Supporting Information

Supplemental experimental procedures, asymmetrical and symmetrical synthetic route for cyanine dyes, MS spectra, HPLC profiles, cell cytotoxicty assay on other gastric cancer cell lines, the toxicity of **CyIC2** in healthy nude mice, the comparsion of specificity and toxicity between **CyIC2-GX1** and **Cy5.5-GX1**, and computational data. This material is available free of charge via the Internet at http://pubs.acs.org.

■ AUTHOR INFORMATION

Corresponding Author

*Tel +86-29-8189-1060, Fax +86-29-8189-1060 (J. Liang); Tel +86-10-6252-7995, Fax +86-10-6252-7995 (J. Tian). E-mail addresses: jimleung@mail.xidian.edu.cn (J. Liang), tian@ieee.org (J. Tian).

Author Contributions

Jing Xin and Xianghan Zhang contributed equally to this work.

Notes

The authors declare no competing financial interest.

■ ACKNOWLEDGMENTS

We gratefully acknowledge Professor Kaichun Wu of the Department of Gastroenterology and State Key Laboratory of Cancer Biology, Xijing Hospital, Fourth Military Medical University for kindly providing us with the GX1 peptide. This work was supported by the Program of the National Basic Research and Development Program of China (973) under Grant No. 2011CB707702, the National Natural Science Foundation of China under Grant Nos. 81090270, 81090272, 81201137, the National Key Technology Support Program under Grant No. 2012BAI23B06, the Natural Science Basic Research Plan in Shaanxi Province of China under Grant No. 2012JC2-10, and the Fundamental Research Funds for the Central Universities.

■ REFERENCES

(1) Luo, S., Zhang, E., Su, Y., Cheng, T., and Shi, C. (2011) A review of NIR dyes in cancer targeting and imaging. *Biomaterials 32*, 7127−7138.

(2) Kosaka, N., Ogawa, M., Choyke, P. L., and Kobayashi, H. (2009) Clinical implications of near-infrared fluorescence imaging in cancer. *Future Oncol. 5*, 1501−1511.

(3) Zhang, C., Liu, T., Su, Y., Luo, S., Zhu, Y., Tan, X., Fan, S., Zhang, L., Zhou, Y., Cheng, T., and Shi, C. (2010) A near-infrared fluorescent heptamethine indocyanine dye with preferential tumor accumulation for in vivo imaging. *Biomaterials 31*, 6612−6617.
(4) Ondrus, A. E., Lee, H. L., Iwanaga, S., Parsons, W. H., Andresen, B. M., Moerner, W. E., and Du Bois, J. (2012) Fluorescent saxitoxins for live cell imaging of single voltage-gated sodium ion channels beyond the optical diffraction limit. *Chem. Biol. 19*, 902−912.
(5) Edgington, L. E., van Raam, B. J., Verdoes, M., Wierschem, C., Salvesen, G. S., and Bogyo, M. (2012) An optimized activity-based probe for the study of caspase-6 activation. *Chem. Biol. 19*, 340−352.
(6) Ramsay, N., Jemth, A. S., Brown, A., Crampton, N., Dear, P., and Holliger, P. (2010) CyDNA: synthesis and replication of highly Cy-dye substituted DNA by an evolved polymerase. *J. Am. Chem. Soc. 132*, 5096−5104.
(7) Gonçalves, M. S. (2009) Fluorescent labeling of biomolecules with organic probes. *Chem. Rev. 109*, 190−212.
(8) Meguellati, K., Koripelly, G., and Ladame, S. (2010) DNA-templated synthesis of trimethine cyanine dyes: a versatile fluorogenic reaction for sensing G-quadruplex formation. *Angew. Chem., Int. Ed. Engl. 49*, 2738−2742.
(9) Lee, H., Mason, J. C., and Achilefu, S. (2008) Synthesis and spectral properties of near-infrared aminophenyl-, hydroxyphenyl-, and phenyl-substituted heptamethine cyanines. *J. Org. Chem. 73*, 723−725.
(10) Lee, H., Akers, W., Bhushan, K., Bloch, S., Sudlow, G., Tang, R., and Achilefu, S. (2011) Near-infrared pH-activatable fluorescent probes for imaging primary and metastatic breast tumors. *Bioconjugate Chem. 22*, 777−784.
(11) Pauli, J., Vag, T., Haag, R., Spieles, M., Wenzel, M., Kaiser, W. A., Resch-Genger, U., and Hilger, I. (2009) An in vitro characterization study of new near infrared dyes for molecular imaging. *Eur. J. Med. Chem. 44*, 3496−3503.
(12) Kobayashi, H., and Choyke, P. L. (2011) Target-cancer-cell-specific activatable fluorescence imaging probes: rational design and in vivo applications. *Acc. Chem. Res. 44*, 83−90.
(13) Lee, S., Xie, J., and Chen, X. (2010) Activatable molecular probes for cancer imaging. *Curr. Top. Med. Chem. 10*, 1135−1144.
(14) Chen, K., and Chen, X. (2010) Design and development of molecular imaging probes. *Curr. Top. Med. Chem. 10*, 1227−1236.
(15) Lee, S., Xie, J., and Chen, X. (2010) Peptide-based probes for targeted molecular imaging. *Biochemistry 49*, 1364−1376.
(16) Ogawa, M., Regino, C. A., Seidel, J., Green, M. V., Xi, W., Williams, M., Kosaka, N., Choyke, P. L., and Kobayashi, H. (2009) Dual-modality molecular imaging using antibodies labeled with activatable fluorescence and a radionuclide for specific and quantitative targeted cancer detection. *Bioconjugate Chem. 20*, 2177−2184.
(17) Shi, H., He, X., Wang, K., Wu, X., Ye, X., Guo, Q., Tan, W., Qing, Z., Yang, X., and Zhou, B. (2011) Activatable aptamer probe for contrast-enhanced in vivo cancer imaging based on cell membrane protein-triggered conformation alteration. *Proc. Natl Acad. Sci. U.S.A. 108*, 3900−3905.
(18) Yu, M. K., Park, J., and Jon, S. (2012) Targeting strategies for multifunctional nanoparticles in cancer imaging and therapy. *Theranostics 2*, 3−44.
(19) Ye, Y., and Chen, X. (2011) Integrin targeting for tumor optical imaging. *Theranostics 1*, 102−126.
(20) Gao, J., Chen, K., Miao, Z., Ren, G., Chen, X., Gambhir, S. S., and Cheng, Z. (2011) Affibody-based nanoprobes for HER2-expressing cell and tumor imaging. *Biomaterials 32*, 2141−2148.
(21) Zhu, L., Niu, G., Fang, X., and Chen, X. (2010) Preclinical molecular imaging of tumor angiogenesis. *Q. J. Nucl. Med. Mol. Imaging 54*, 291−308.
(22) Chen, K., Yap, L. P., Park, R., Hui, X., Wu, K., Fan, D., Chen, X., and Conti, P. S. (2012) A Cy5.5-labeled phage-displayed peptide probe for near-infrared fluorescence imaging of tumor vasculature in living mice. *Amino Acids 42*, 1329−1337.
(23) Folkman, J. (2002) Role of angiogenesis in tumor growth and metastasis. *Semin. Oncol. 29*, 15−18.
(24) Hui, X., Han, Y., Liang, S., Liu, Z., Liu, J., Hong, L., Zhao, L., He, L., Cao, S., Chen, B., Yan, K., Jin, B., Chai, N., Wang, J., Wu, K., and Fan, D. (2008) Specific targeting of the vasculature of gastric cancer by a new tumor-homing peptide CGNSNPKSC. *J. Controlled Release 131*, 86−93.
(25) Zhi, M., Wu, K. C., Dong, L., Hao, Z. M., Deng, T. Z., Hong, L., Liang, S. H., Zhao, P. T., Qiao, T. D., Wang, Y., Xu, X., and Fan, D. M. (2004) Characterization of a specific phage-displayed peptide binding to vasculature of human gastric cancer. *Cancer Biol. Ther. 3*, 1232−1235.
(26) Khodarev, N. N., Yu, J., Labay, E., Darga, T., Brown, C. K., Mauceri, H. J., Yassari, R., Gupta, N., and Weichselbaum, R. R. (2003) Tumour-endothelium interactions in co-culture: coordinated changes of gene expression profiles and phenotypic properties of endothelial cells. *J. Cell. Sci. 116*, 1013−1022.
(27) Mujumdar, R. B., Ernst, L. A., Mujumdar, S. R., Lewis, C. J., and Waggoner, A. S. (1993) Cyanine dye labeling reagents: sulfoindocyanine succinimidyl esters. *Bioconjugate Chem. 4*, 105−111.
(28) Bouteiller, C., Clavé, G., Bernardin, A., Chipon, B., Massonneau, M., Renard, P. Y., and Romieu, A. (2007) Novel water-soluble near-infrared cyanine dyes: synthesis, spectral properties, and use in the preparation of internally quenched fluorescent probes. *Bioconjugate Chem. 18*, 1303−1317.
(29) Peng, X. J., Yang, Z. G., Wang, J. Y., Fan, J. L., He, Y. X., Song, F. L., Wang, B. S., Sun, S. G., Qu, J. L., Qi, J., and Yan, M. (2011) Fluorescence ratiometry and fluorescence lifetime imaging: using a single molecular sensor for dual mode imaging of cellular viscosity. *J. Am. Chem. Soc. 133*, 6626−6635.
(30) Becke, A. D. (1993) Density-functional thermochemistry. III.The role of exact exchange. *J. Chem. Phys. 98*, 5648−5642.
(31) Song, B., Zhang, Q., Ma, W. H., Peng, X. J., Fu, X. M., and Wang, B. S. (2009) The synthesis and photostability of novel squarylium indocyanine dyes. *Dyes Pigm. 82*, 396−400.